Viscous contributions to the pressure for potential flow analysis of capillary instability of two viscous fluids

J. Wang and D. D. Joseph[a)]
Department of Aerospace Engineering and Mechanics, University of Minnesota, Minneapolis, Minnesota 55455

T. Funada
Department of Digital Engineering, Numazu College of Technology, 3600 Ooka, Numazu, Shizuoka 410-8501, Japan

(Received 29 July 2004; accepted 17 February 2005; published online 2 May 2005)

Capillary instability of a liquid cylinder immersed in another liquid is analyzed using viscous potential flow. An effect of viscosity on the irrotational motion may be introduced by evaluating the viscous normal stress at the liquid–liquid interface on the irrotational motions. In a second approximation, the explicit effects of the discontinuity of the shear stress and tangential component of velocity which cannot be resolved pointwise in irrotational flows, can be removed in the mean from the power of traction integrals in the energy equation by the selection of two viscous corrections of the irrotational pressure. The actual resolution of these discontinuities presumably takes place in a boundary layer which is not computed or needed. We include the irrotational stress and pressure correction in the normal stress balance and compare the computed growth rates to the growth rates of the exact viscous flow solution. The agreement is excellent when one of the liquids is a gas; for two viscous liquids, the agreement is good to reasonable for the maximum growth rates but poor for long waves. Calculations show that good agreement is obtained when the vorticity is relatively small or the irrotational part is dominant in the exact viscous solution. We show that the irrotational viscous flow with pressure corrections gives rise to exactly the same dispersion relation as the dissipation method in which no pressure at all is required and the viscous effect is accounted for by evaluating the viscous dissipation using the irrotational flow. © *2005 American Institute of Physics*. [DOI: 10.1063/1.1914573]

I. INTRODUCTION

A liquid thread of mean radius R immersed in another liquid is subject to capillary instability. The capillary collapse can be described as a neck-down due to the surface tension γ in which the liquid is ejected from the throat of the neck, as seen in Fig. 1. Capillary instability is responsible for drop formation in applications such as ink-jet printing, fiber spinning, and silicon chip technology.

The dynamical theory of instability of a long cylindrical column of liquid of radius R under the action of capillary force was given by Rayleigh[1] following earlier work by Plateau[2] who showed that a long cylinder of liquid is unstable to disturbances with wavelengths greater than $2\pi R$. Rayleigh showed that the effect of inertia is such that the wavelength λ corresponding to the mode of maximum instability is $\lambda = 4.51 \times 2R$, exceeding considerably the circumference of the cylinder. The idea that the wavelength associated with fastest growing growth rate would become dominant and be observed in practice was first put forward by Rayleigh.[1] The analysis of Rayleigh is based on potential flow of an inviscid liquid neglecting the effect of the outside fluid. An attempt to account for viscous effects was made by Rayleigh[3] again neglecting the effect of the surrounding fluid. One of the effects considered is meant to account for the forward motion of an inviscid fluid with a resistance proportional to velocity. The effect of viscosity is treated in the special case in which the viscosity is so great that inertia may be neglected. He showed that the wavelength for maximum growth is very large, strictly infinite. Weber[4] extended Rayleigh's theory by considering an effect of viscosity and that of surrounding air on the stability of a columnar jet. The effect of viscosity on the stability of a liquid cylinder when the surrounding fluid is neglected and on a hollow (dynamically passive) cylinder in a viscous liquid was treated briefly by Chandrasekhar.[5] Eggers[6] has given a comprehensive review of nonlinear dynamics and breakup of free surface flows.

Tomotika[7] studied capillary instability and gave an exact normal mode solution of the linearized Navier–Stokes equations. Funada and Joseph[8] analyzed the same problem assuming that the flow is irrotational. In their potential flow analyses, the growth rate of the instability is obtained by considering the normal stress balance at the interface. If the viscosities of the liquids are ignored and only the irrotational pressure and capillary force enter the balance, the analysis is called an inviscid potential flow analysis (IPF). If the viscous stress is included in the normal stress balance, the analysis is called a viscous potential flow analysis (VPF). Funada and Joseph[8] showed that the growth rates computed using VPF are more accurate than using IPF.

[a)]Author to whom correspondence should be addressed. Telephone: (612) 625-0309. Fax: (612) 626-1558. Electronic mail: joseph@aem.umn.edu

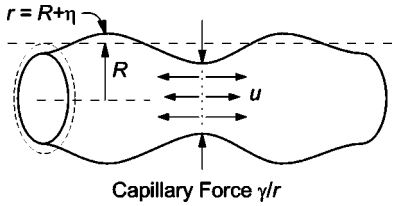

FIG. 1. Capillary instability. The force γ/r drives fluid away from the throat, leading to collapse.

Wang, Joseph, and Funada[9] computed a viscous correction of the irrotational pressure using a formulation proposed by Joseph and Wang.[10] This viscous correction of VPF, called VCVPF, is also an irrotational flow which differs from VPF only by the additional viscous pressures. These additional pressures are presumably induced in a boundary layer by the discrepancy between the nonzero irrotational shear stress and the zero-shear-stress condition at a free surface. The boundary layer is not studied and is not needed in determining the pressure correction. Wang, Joseph, and Funada[9] considered capillary instability in cases in which one liquid is viscous and the other is a gas of negligible density and viscosity. They included the pressure correction in the normal stress balance at the free surface and showed that the growth rates computed using VCVPF are almost indistinguishable from the exact solution.

Here, we extend the VCVPF analysis to cases involving the interface of two viscous fluids. The formulation for the pressure correction is derived and used to compute growth rates for capillary instability of two viscous fluids. The computed values of the maximum growth rate and the associated wave number computed from VCVPF are close to those from the exact solution; but the growth rates at small wave numbers are not in good agreement.

Another way to obtain a viscous correction of VPF is by evaluating the viscous dissipation in the liquid using the irrotational flow. The dissipation method was introduced by Lamb[11] in his study of the effect of viscosity on the decay of irrotational waves on water. We carry out the dissipation calculation for the capillary instability of two viscous fluids and show that the growth rates are the same as from VCVPF.

Our theory of VCVPF is a purely irrotational approximation to the exact viscous solution. Other approximations for interfacial flows have been studied by many investigators in the context of drop oscillations (Lamb,[11] Miller and Scriven,[12] Prosperetti,[13] Lundgren and Mansour[14]). Miller and Scriven[12] studied the oscillation of a liquid droplet immersed in another fluid. They found that the approximation based on irrotational profiles is adequate when the interface is free and either the interior or exterior fluid is a gas of negligible density and viscosity. When the viscosities of the two fluids are comparable, the viscous dissipation in the boundary layer near the interface gives significant contribution to the damping rate of the oscillation. The irrotational flows, which do not account for the boundary-layer flow, do not lead to a good approximations of the damping rate. Miller and Scriven's conclusions are generally consistent with our results for capillary instability: the agreement between VCVPF and the exact solution is remarkably good in gas–liquid cases; it is not as good in liquid–liquid cases, but a reasonable approximation can still be obtained from the purely irrotational solution in a neighborhood of the maximum growth rate.

II. LINEARIZED EQUATIONS GOVERNING CAPILLARY INSTABILITY

Consider the stability of a liquid cylinder of radius R with viscosity μ_l and density ρ_l surrounded by another fluid with viscosity μ_a and density ρ_a under capillary forces generated by interfacial tension γ. Note that we use the subscript "l" for the inside fluid and "a" for the outside fluid. The analysis is done in cylindrical coordinates (r,θ,z) and only axisymmetric disturbances independent of θ are considered. The linearized Navier–Stokes equations and interfacial conditions are made dimensionless with the following scales:

$$[\text{length},\text{velocity},\text{time},\text{pressure}]=[D,U,D/U,p_0],$$

where D is the diameter of the liquid cylinder, $U=\sqrt{\gamma/(\rho_l D)}$, $p_0=\rho_l U^2=\gamma/D$. The three dimensionless parameters controlling the solution are $m=\mu_a/\mu_l$, $l=\rho_a/\rho_l$, and a Reynolds number $J=VD\rho_l/\mu_l=\mathrm{Oh}^2$ where $V=\gamma/\mu_l$ and Oh is the Ohnesorge number. The governing equations are

$$\frac{\partial u_l}{\partial r}+\frac{u_l}{r}+\frac{\partial w_l}{\partial z}=0, \tag{1}$$

$$\frac{\partial u_l}{\partial t}=-\frac{\partial p_l}{\partial r}+\frac{1}{\sqrt{J}}\left(\nabla^2 u_l-\frac{u_l}{r^2}\right),\quad \frac{\partial w_l}{\partial t}=-\frac{\partial p_l}{\partial z}+\frac{1}{\sqrt{J}}\nabla^2 w_l, \tag{2}$$

$$\frac{\partial u_a}{\partial r}+\frac{u_a}{r}+\frac{\partial w_a}{\partial z}=0, \tag{3}$$

$$l\frac{\partial u_a}{\partial t}=-\frac{\partial p_a}{\partial r}+\frac{m}{\sqrt{J}}\left(\nabla^2 u_a-\frac{u_a}{r^2}\right),$$

$$l\frac{\partial w_a}{\partial t}=-\frac{\partial p_a}{\partial z}+\frac{m}{\sqrt{J}}\nabla^2 w_a, \tag{4}$$

with $\nabla^2=(\partial^2/\partial r^2)+(1/r)(\partial/\partial r)+(\partial^2/\partial z^2)$. The kinematic condition at the interface $r=1/2+\eta$ (where η is the varicose displacement) is given by

$$\frac{\partial \eta}{\partial t}=u_l,\quad \frac{\partial \eta}{\partial t}=u_a. \tag{5}$$

The normal stress balance at the interface is given by

$$p_a-p_l+\frac{2}{\sqrt{J}}\frac{\partial u_l}{\partial r}-\frac{2m}{\sqrt{J}}\frac{\partial u_a}{\partial r}=\frac{\partial^2\eta}{\partial z^2}+\frac{\eta}{R^2}. \tag{6}$$

The tangential stress balance at the interface is given by

$$\left(\frac{\partial u_l}{\partial z}+\frac{\partial w_l}{\partial r}\right)=m\left(\frac{\partial u_a}{\partial z}+\frac{\partial w_a}{\partial r}\right). \tag{7}$$

The continuity of the velocity at the interface requires

$$u_l = u_a, \tag{8}$$

$$w_l = w_a. \tag{9}$$

III. FULLY VISCOUS FLOW ANALYSIS

Tomotika[7] gave a normal mode solution to the linearized governing equations. This is an exact solution which satisfies all the four interfacial conditions in (6)–(9). He expressed the velocities with a stream function $\psi(r,z,t)$,

$$u = \frac{1}{r}\frac{\partial \psi}{\partial z}, \quad w = -\frac{1}{r}\frac{\partial \psi}{\partial r}, \tag{10}$$

and the basic variables are expressed in normal modes,

$$\psi_l = [A_1 r I_1(kr) + A_2 r I_1(k_l r)]\exp(\sigma t + \mathrm{i}kz), \tag{11}$$

$$\psi_a = [B_1 r K_1(kr) + B_2 r K_1(k_a r)]\exp(\sigma t + \mathrm{i}kz), \tag{12}$$

$$\eta = H\exp(\sigma t + \mathrm{i}kz), \tag{13}$$

where σ is the complex growth rate and k is the wave number; the modified Bessel functions of the first order are denoted by I_1 for the first kind and K_1 for the second kind. Substitution of (11)–(13) to (6)–(9) leads to the solvability condition, which is given as the dispersion relation,

$$\begin{vmatrix} I_1(kR) & I_1(k_lR) & K_1(kR) & K_1(k_aR) \\ kI_0(kR) & k_lI_0(k_lR) & -kK_0(kR) & -k_aK_0(k_aR) \\ 2k^2I_1(kR) & (k^2+k_l^2)I_1(k_lR) & 2mk^2K_1(kR) & m(k^2+k_a^2)K_1(k_aR) \\ F_1 & F_2 & F_3 & F_4 \end{vmatrix} = 0, \tag{14}$$

where

$$F_1 = i\sigma I_0(kR) + 2i\frac{k^2}{\sqrt{J}}\left(\frac{dI_1(kR)}{d(kR)}\right) - \left(\frac{1}{R^2} - k^2\right)i\frac{k}{\sigma}I_1(kR), \tag{15}$$

$$F_2 = 2i\frac{kk_l}{\sqrt{J}}\left(\frac{dI_1(k_lR)}{d(k_lR)}\right) - \left(\frac{1}{R^2} - k^2\right)i\frac{k}{\sigma}I_1(k_lR), \tag{16}$$

$$F_3 = -il\sigma K_0(kR) + 2i\frac{mk^2}{\sqrt{J}}\left(\frac{dK_1(kR)}{d(kR)}\right), \tag{17}$$

$$F_4 = 2i\frac{mkk_a}{\sqrt{J}}\left(\frac{dK_1(k_aR)}{d(k_aR)}\right),$$

with

$$k_l = (k^2 + \sqrt{J}\sigma)^{1/2}, \quad k_a = \left(k^2 + \frac{l}{m}\sqrt{J}\sigma\right)^{1/2}. \tag{18}$$

IV. VISCOUS POTENTIAL FLOW ANALYSIS

The potential flow solution (Funada and Joseph[8]) is given by $\mathbf{u} = \nabla\phi$, $\nabla^2\phi = 0$, where ϕ is the velocity potential. The normal stress balance (6) and normal velocity continuity (8) are satisfied; the shear stress and tangential velocity conditions (7) and (9) cannot be enforced. The potential solution can be expressed as

$$\psi_l = A_1 r I_1(kr)\exp(\sigma t + ikz), \tag{19}$$

$$\psi_a = B_1 r K_1(kr)\exp(\sigma t + ikz), \tag{20}$$

$$\eta = H\exp(\sigma t + ikz), \tag{21}$$

for which the dispersion relation is given by

$$(\alpha_l + l\alpha_a)\sigma^2 + \frac{2k^2}{\sqrt{J}}(\beta_l + m\beta_a)\sigma = \left(\frac{1}{R^2} - k^2\right)k, \tag{22}$$

with

$$\alpha_l = \frac{I_0(kR)}{I_1(kR)}, \quad \alpha_a = \frac{K_0(kR)}{K_1(kR)}, \quad \beta_l = \alpha_l - \frac{1}{kR}, \quad \beta_a = \alpha_a + \frac{1}{kR}. \tag{23}$$

Solving (22), we obtain

$$\sigma = -\frac{k^2(\beta_l + m\beta_a)}{\sqrt{J}(\alpha_l + l\alpha_a)} \pm \left\{\left[\frac{k^2(\beta_l + m\beta_a)}{\sqrt{J}(\alpha_l + l\alpha_a)}\right]^2 + \left(\frac{1}{R^2} - k^2\right)\frac{k}{\alpha_l + l\alpha_a}\right\}^{1/2}. \tag{24}$$

Thus instability arises in $0 < kR < 1$, for which the dimensionless critical wave number $k_c = 1/R = 2$. When $\sqrt{J} \to \infty$, (24) reduces to

$$\sigma = \pm\sqrt{\left(\frac{1}{R^2} - k^2\right)\frac{k}{\alpha_l + l\alpha_a}}, \tag{25}$$

which is just the dispersion relation in IPF; the same dispersion relation was obtained by Christiansen and Hixson.[15]

V. PRESSURE CORRECTION FOR VISCOUS POTENTIAL FLOW

Joseph and Wang[10] derived a viscous correction for the irrotational pressure at free surfaces of steady flows, which is induced by the discrepancy between the nonzero irrotational shear stress and the zero-shear-stress condition at free surfaces. In the VPF analysis of capillary instability, the interface between two viscous fluids is involved and the two potential flows are unsteady. We will derive the pressure correction for capillary instability from the basic mechanical energy equation.

If we ignore the small deformation η in the linear problem, we have $\mathbf{n}_1=\mathbf{e}_r$ as the outward normal at the interface for the inside fluid; $\boldsymbol{n}_2=-\boldsymbol{n}_1$ is the outward normal for the outside fluid; $\boldsymbol{t}=\boldsymbol{e}_z$ is the unit tangential vector. We use the superscript "i" for "irrotational" and "v" for "viscous." The normal and shear parts of the viscous stress are represented by τ^n and τ^s, respectively.

The velocities and stresses are evaluated using the potentials, which are expressed by stream functions (19) and (20). The mechanical energy equations for the outside and inside fluids are, respectively,

$$\frac{d}{dt}\int_{V_a}\frac{\rho_a}{2}|\boldsymbol{u}_a|^2dV=\int_A[\boldsymbol{u}_a\cdot\mathbf{T}_a\cdot\boldsymbol{n}_2]dA-\int_{V_a}2\mu_a\mathbf{D}_a{:}\mathbf{D}_adV$$
$$=-\int_A[\boldsymbol{u}_a\cdot\boldsymbol{n}_1(-p_a^i+\tau_a^n)+\boldsymbol{u}_a\cdot\boldsymbol{t}\tau_a^s]dA-\int_{V_a}2\mu_a\mathbf{D}_a{:}\mathbf{D}_adV, \tag{26}$$

$$\frac{d}{dt}\int_{V_l}\frac{\rho_l}{2}|\boldsymbol{u}_l|^2dV=\int_A[\boldsymbol{u}_l\cdot\mathbf{T}_l\cdot\boldsymbol{n}_1]dA-\int_{V_l}2\mu_l\mathbf{D}_l{:}\mathbf{D}_ldV$$
$$=\int_A[\boldsymbol{u}_l\cdot\boldsymbol{n}_1(-p_l^i+\tau_l^n)+\boldsymbol{u}_l\cdot\boldsymbol{t}\tau_l^s]dA-\int_{V_l}2\mu_l\mathbf{D}_l{:}\mathbf{D}_ldV. \tag{27}$$

With the continuity of the normal velocity

$$\boldsymbol{u}_a\cdot\boldsymbol{n}_1=\boldsymbol{u}_l\cdot\boldsymbol{n}_1=u_n, \tag{28}$$

the sum of (26) and (27) can be written as

$$\frac{d}{dt}\int_{V_a}\frac{\rho_a}{2}|\boldsymbol{u}_a|^2dV+\frac{d}{dt}\int_{V_l}\frac{\rho_l}{2}|\boldsymbol{u}_l|^2dV$$
$$=\int_A[u_n(-p_l^i+\tau_l^n+p_a^i-\tau_a^n)+\boldsymbol{u}_l\cdot\boldsymbol{t}\tau_l^s-\boldsymbol{u}_a\cdot\boldsymbol{t}\tau_a^s]dA-\int_{V_a}2\mu_a\mathbf{D}_a{:}\mathbf{D}_adV-\int_{V_l}2\mu_l\mathbf{D}_l{:}\mathbf{D}_ldV. \tag{29}$$

Now consider the boundary layer approximation of viscous potential flow. We propose two pressure corrections, p_l^v and p_a^v, for the inside and outside potential flows, respectively, together with the continuity conditions

$$\tau_a^s=\tau_l^s=\tau^s,\quad \boldsymbol{u}_a\cdot\boldsymbol{t}=\boldsymbol{u}_l\cdot\boldsymbol{t}=u_s. \tag{30}$$

We assume that the boundary layer approximation has a negligible effect on the flow in the bulk liquid but it changes the pressure and continuity conditions at the interface. Hence, the mechanical energy equations become

$$\frac{d}{dt}\int_{V_l}\frac{\rho_l}{2}|\boldsymbol{u}_l|^2dV=\int_A[u_n(-p_l^i-p_l^v+\tau_l^n)+u_s\tau^s]dA-\int_{V_l}2\mu_l\mathbf{D}_l{:}\mathbf{D}_ldV, \tag{31}$$

$$\frac{d}{dt}\int_{V_a}\frac{\rho_a}{2}|\boldsymbol{u}_a|^2dV=-\int_A[u_n(-p_a^i-p_a^v+\tau_a^n)+u_s\tau^s]dA-\int_{V_a}2\mu_a\mathbf{D}_a{:}\mathbf{D}_adV. \tag{32}$$

The sum of (31) and (32) can be written as

$$\frac{d}{dt}\int_{V_a}\frac{\rho_a}{2}|\boldsymbol{u}_a|^2dV+\frac{d}{dt}\int_{V_l}\frac{\rho_l}{2}|\boldsymbol{u}_l|^2dV$$
$$=\int_A[u_n(-p_l^i-p_l^v+\tau_l^n+p_a^i+p_a^v-\tau_a^n)]dA-\int_{V_a}2\mu_a\mathbf{D}_a{:}\mathbf{D}_adV-\int_{V_l}2\mu_l\mathbf{D}_l{:}\mathbf{D}_ldV. \tag{33}$$

Comparing (29) and (33), we obtain an equation which relates the pressure corrections to the uncompensated irrotational shear stresses

$$\int_A u_n(-p_l^v+p_a^v)dA=\int_A(\boldsymbol{u}_l\cdot\boldsymbol{t}\tau_l^s-\boldsymbol{u}_a\cdot\boldsymbol{t}\tau_a^s)dA. \tag{34}$$

Joseph and Wang[10] showed that in linearized problems, the governing equation for the pressure corrections is

$$\nabla^2p^v=0. \tag{35}$$

Solving Eq. (35), we obtain the two pressure corrections,

$$-p_l^v=\sum_{j=0}^{\infty}C_j'iI_0\left(\frac{2\pi}{\lambda}jr\right)\exp\left(\sigma t+i\frac{2\pi}{\lambda}jz\right), \tag{36}$$

$$-p_a^v=\sum_{j=0}^{\infty}D_j'iK_0\left(\frac{2\pi}{\lambda}jr\right)\exp\left(\sigma t+i\frac{2\pi}{\lambda}jz\right), \tag{37}$$

where C_j' and D_j' are constants to be determined, j is an integer, and λ is the period in z direction. Suppose $2\pi j_0/\lambda=k$, $C_{j_0}'=C_k$, and $D_{j_0}'=D_k$, then the two pressure corrections can be written as

$$-p_l^v=C_kiI_0(kr)\exp(\sigma t+ikz)+\sum_{j\neq j_0}C_j'iI_0\left(\frac{2\pi}{\lambda}jr\right)\exp\left(\sigma t+i\frac{2\pi}{\lambda}jz\right), \tag{38}$$

$$-p_a^v = D_k i K_0(kr)\exp(\sigma t + ikz) + \sum_{j\neq j_0} D_j' i K_0\left(\frac{2\pi}{\lambda} jr\right)\exp\left(\sigma t + i\frac{2\pi}{\lambda} jz\right). \tag{39}$$

With the pressure corrections, the normal stress balance has the following form:

$$p_a^i + p_a^v - p_l^i - p_l^v + \frac{2}{\sqrt{J}}\frac{\partial u_l}{\partial r} - \frac{2m}{\sqrt{J}}\frac{\partial u_a}{\partial r} = \frac{\partial^2 \eta}{\partial z^2} + \frac{\eta}{R^2}, \tag{40}$$

which gives rise to

$$\begin{aligned}&\left\{ lB_1 K_0(kR)\sigma - D_k K_0(kR) + A_1\sigma I_0(kR) + C_k I_0(kR) \right.\\ &\quad + \frac{2k^2}{\sqrt{J}} A_1\left[I_0(kR) - \frac{I_1(kR)}{kR}\right]\\ &\quad \left. + \frac{2mk^2}{\sqrt{J}} B_1\left[K_0(kR) + \frac{K_1(kR)}{kR}\right]\right\}\exp(\sigma t + ikz)\\ &\quad + \sum_{j\neq j_0}\left[C_j' I_0\left(\frac{2\pi}{\lambda} jR\right) - D_j' K_0\left(\frac{2\pi}{\lambda} jR\right)\right]\\ &\quad \times\exp\left(\sigma t + i\frac{2\pi}{\lambda} jz\right)\\ &\quad = A_1\frac{k}{\sigma} I_1(kR)\left(\frac{1}{R^2} - k^2\right)\exp(\sigma t + ikz).\end{aligned} \tag{41}$$

By orthogonality of the Fourier series, we obtain

$$\begin{aligned}&lB_1 K_0(kR)\sigma - D_k K_0(kR) + A_1\sigma I_0(kR) + C_k I_0(kR)\\ &\quad + \frac{2k^2}{\sqrt{J}} A_1\left[I_0(kR) - \frac{I_1(kR)}{kR}\right]\\ &\quad + \frac{2mk^2}{\sqrt{J}} B_1\left[K_0(kR) + \frac{K_1(kR)}{kR}\right]\\ &\quad = A_1\frac{k}{\sigma} I_1(kR)\left(\frac{1}{R^2} - k^2\right),\end{aligned} \tag{42}$$

and

$$C_j' I_0\left(\frac{2\pi}{\lambda} jR\right) - D_j' K_0\left(\frac{2\pi}{\lambda} jR\right) = 0 \quad \text{when } j \neq j_0. \tag{43}$$

Equation (42) replaces the normal stress balance and can be solved for the growth rate σ. However, the undetermined part $C_k I_0(kR) - D_k K_0(kR)$ has to be computed from (34) before we can solve (42). Substitution of (38), (39), and (43) into the left-hand side of (34) gives rise to

$$\begin{aligned}\int_A \overline{u_n}(-p_l^v + p_a^v)dA &= \int_0^{2\pi} R\, d\theta \int_z^{z+\lambda} \overline{u_n}(-p_l^v + p_a^v)dz\\ &= 2\pi R\lambda[\overline{A_1} C_k I_0(kR) I_1(kR)\\ &\quad - \overline{B_1} D_k K_0(kR) K_1(kR)]k\\ &\quad \times\exp(\sigma + \overline{\sigma})t,\end{aligned} \tag{44}$$

where $\overline{u_n}$ is the conjugate of u_n. The right-hand side of (34) can be evaluated,

$$\begin{aligned}\int_A [(\overline{\boldsymbol{u}_l\cdot\boldsymbol{t}})\tau_l^s - (\overline{\boldsymbol{u}_a\cdot\boldsymbol{t}})\tau_a^s]dA &= \frac{4\pi R\lambda}{\sqrt{J}}[\overline{A_1} A_1 I_0(kR) I_1(kR)\\ &\quad + m\overline{B_1} B_1 K_0(kR) K_1(kR)]k^3\\ &\quad \times\exp(\sigma + \overline{\sigma})t.\end{aligned} \tag{45}$$

Combining (44) and (45), we obtain

$$\begin{aligned}&\overline{A_1} C_k I_0(kR) I_1(kR) - \overline{B_1} D_k K_0(kR) K_1(kR)\\ &\quad = \frac{2}{\sqrt{J}} A_1 A_1 k^2 I_0(kR) I_1(kR) + \frac{2m}{\sqrt{J}}\overline{B_1} B_1 k^2 K_0(kR) K_1(kR).\end{aligned} \tag{46}$$

The normal velocity continuity condition (28) leads to

$$B_1 = A_1\frac{I_1(kR)}{K_1(kR)}. \tag{47}$$

Substitution of (47) into (46) leads to

$$\begin{aligned}C_k I_0(kR) - D_k K_0(kR) &= \frac{2}{\sqrt{J}} A_1 k^2 I_0(kR)\\ &\quad + \frac{2m}{\sqrt{J}} A_1 k^2 I_1(kR) K_0(kR)/K_1(kR).\end{aligned} \tag{48}$$

Inserting (47) and (48) into (42), we obtain the dispersion relation

$$\begin{aligned}&(\alpha_l + l\alpha_a)\sigma^2 + \frac{2k^2}{\sqrt{J}}[(\alpha_l + \beta_l) + m(\alpha_a + \beta_a)]\sigma\\ &\quad = \left(\frac{1}{R^2} - k^2\right)k,\end{aligned} \tag{49}$$

where α_l, α_a, β_a, and β_l are defined in (23). Solving (49), we obtain the growth rate

$$\begin{aligned}\sigma = &-\frac{k^2[(\alpha_l + \beta_l) + m(\alpha_a + \beta_a)]}{\sqrt{J}(\alpha_l + l\alpha_a)}\\ &\pm\left\{\left[\frac{k^2[(\alpha_l + \beta_l) + m(\alpha_a + \beta_a)]}{\sqrt{J}(\alpha_l + l\alpha_a)}\right]^2\right.\\ &\left. + \left(\frac{1}{R^2} - k^2\right)\frac{k}{\alpha_l + l\alpha_a}\right\}^{1/2}.\end{aligned} \tag{50}$$

VI. COMPARISON OF GROWTH RATES

We calculate the growth rate σ using IPF (25), VPF (24), and VCVPF (50) and compare these results with the exact solution (14). We choose five pairs of fluids to study capillary instability and the properties of the fluids, and controlling dimensionless parameters are listed in Table I.

We are essentially comparing solutions assuming irrotational flows to the exact solution. To better understand the potential flow approximation to the fully viscous flow, we may evaluate the vorticity,

TABLE I. The properties of the five pairs of fluids used to study capillary instability and the controlling dimensionless parameters l, m, and J.

Case	1	2	3	4	5
Fluids	Mercury-water	Water-benzene	Glycerin-mercury	Goldensyrup-paraffin	Goldensyrup-BBoil
ρ_l (kg m^{-3})	13 500	1000	1 257	1400	1400
ρ_a (kg m^{-3})	1 000	0.001	13 500	1600	900
μ_l (kg/m s)	0.001 56	860	0.782	11.0	11.0
μ_a (kg/m s)	0.001	0.000 65	0.001 56	0.0034	6.0
γ (N/m)	0.375	0.032 8	0.375	0.023	0.017
$l=\rho_a/\rho_l$	0.074 07	0.86	10.74	1.143	0.6429
$m=\mu_a/\mu_l$	0.641 0	0.65	1.995×10^{-3}	3.091×10^{-4}	0.5455
$J=\rho_l\gamma D/\mu_l^2$	2.080×10^{7}	3.280×10^{5}	7.708	2.661×10^{-3}	1.967×10^{-3}

$$\omega=\frac{\partial u_r}{\partial z}-\frac{\partial u_z}{\partial r}=\frac{\partial u}{\partial z}-\frac{\partial w}{\partial r}, \tag{51}$$

in the interior and exterior fluids from the exact solution. When the vorticity is great, the potential flow cannot give a satisfactory approximation.

The vorticity is

$$\begin{aligned}\omega_l &= A_2 I_1(k_l r)(k_l^2-k^2)\exp(\sigma t+ikz)\\ &= A_2 I_1(k_l r)\sqrt{J}\sigma\exp(\sigma t+ikz)\end{aligned} \tag{52}$$

in the interior fluid and is

$$\begin{aligned}\omega_a &= B_2 K_1(k_a r)(k_a^2-k^2)\exp(\sigma t+ikz)\\ &= B_2 K_1(k_a r)\frac{l}{m}\sqrt{J}\sigma\exp(\sigma t+ikz)\end{aligned} \tag{53}$$

in the exterior fluid. The magnitudes of ω_l and ω_a are proportional to A_2 and B_2, respectively. We normalize them by B_2 so that the two magnitudes are measured by the same scale and can be compared. The normalized magnitudes of the vorticities at the interface ($r\approx R$) are

$$\omega_l^*=-\frac{A_2}{B_2}I_1(k_l R)\sqrt{J}\sigma,\quad \omega_a^*=K_1(k_a R)\frac{l}{m}\sqrt{J}\sigma. \tag{54}$$

Note that we add a minus sign for ω_l^*. The reason is that the vorticity vectors in the interior and exterior fluids are in opposite directions, leading to vorticities of opposite signs. By adding a minus sign for ω_l^*, we obtain the absolute value of the vorticity in the interior fluid. To compute (54), we need to know the value of A_2/B_2. This can be achieved by manipulation of the dispersion relation (14),

$$\begin{bmatrix} I_1(kR) & I_1(k_lR) & K_1(kR)\\ kI_0(kR) & k_lI_0(k_lR) & -kK_0(kR)\\ 2k^2I_1(kR) & (k^2+k_l^2)I_1(k_lR) & 2mk^2K_1(kR)\end{bmatrix}\begin{bmatrix}A_1/B_2\\ A_2/B_2\\ B_1/B_2\end{bmatrix} = \begin{bmatrix}-K_1(k_aR)\\ k_aK_0(k_aR)\\ -m(k^2+k_a^2)K_1(k_aR)\end{bmatrix}, \tag{55}$$

from which we can solve for A_1/B_2, A_2/B_2, and B_1/B_2.

We note that the stream functions (11) and (12) in the exact solution can be divided into the irrotational part and rotational part:

$$\begin{aligned}\psi_l^i &= A_1 r I_1(kr)\exp(\sigma t+ikz),\\ \psi_l^r &= A_2 r I_1(k_l r)\exp(\sigma t+ikz);\end{aligned} \tag{56}$$

$$\begin{aligned}\psi_a^i &= B_1 r K_1(kr)\exp(\sigma t+ikz),\\ \psi_a^r &= B_2 r K_1(k_a r)\exp(\sigma t+ikz).\end{aligned} \tag{57}$$

The irrotational parts are exactly the potential flow solution, whereas the vorticities are solely determined by the rotational parts. When the irrotational parts dominate, potential flows can give good approximation to the exact solution; when the rotational parts are important, the approximation cannot be satisfactory. We define two ratios of the irrotational part to the rotational part:

$$f_l=\left|\frac{\psi_l^i(r=R)}{\psi_l^r(r=R)}\right|=\left|\frac{A_1I_1(kR)}{A_2I_1(k_lR)}\right|, \tag{58}$$

$$f_a=\left|\frac{\psi_a^i(r=R)}{\psi_a^r(r=R)}\right|=\left|\frac{B_1K_1(kR)}{B_2K_1(k_aR)}\right|. \tag{59}$$

These two ratios characterize the relative importance of the irrotational and rotational parts at the interface. When the Reynolds number is large, we expect the values of the ratios to be high.

We present the comparison of the growth rates computed from IPF, VPF, VCVPF, and the exact solution in Figs. 2–6 for the five pairs of fluids listed in Table I. In each case, a growth rate vs wave-number plot, a vorticity vs wave-number plot, and a plot for the two ratios f_l and f_a vs wave number are shown. The vorticity plot and the plot for the two ratios can help to understand the agreement and disagreement between the growth rates from potential-based solutions and from the exact solution.

When the Reynolds number is high (Figs. 2 and 3), the three potential flow based solutions are essentially the same; they are in good agreement with the exact solution in the maximum growth region (see Table II) but deviate from the

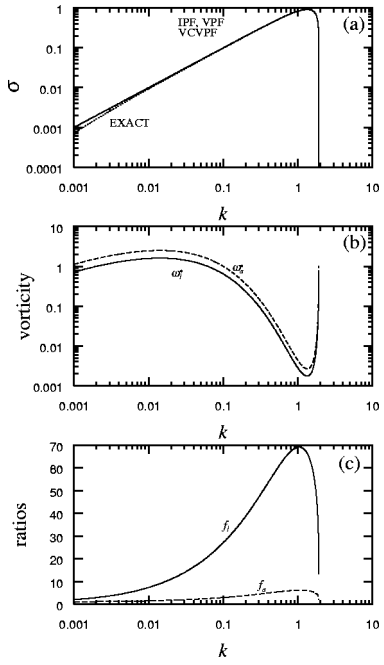

FIG. 2. (a) The growth rate σ vs k for case 1, mercury in water. The three potential-flow-based analyses agree with the exact solution well but deviate from it slightly when $k \ll 1$. (b) The vorticities ω_l^* and ω_a^* vs k for case 1. The magnitude of the vorticity is large when $k \ll 1$ and small when k is about 1. (c) The two ratios f_l and f_a vs k for case 1. The irrotational parts dominate when k is close to 1; the irrotational and rotational parts are comparable when $k \ll 1$ or $k \approx 2$. The dominance of the irrotational part in the maximum growth region is understandable because the Reynolds number is very high, 2.080×10^7. Both the vorticities and the two ratios could help to understand the deviation of the potential based analyses from the exact solution when $k \ll 1$.

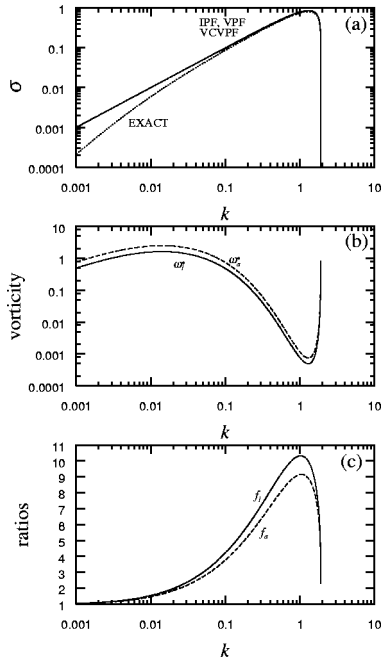

FIG. 3. (a) The growth rate σ vs k for case 2, water in benzene. The three potential-flow-based analyses agree with the exact solution in the maximum growth region but deviate from it considerably when k is small. (b) The vorticities ω_l^* and ω_a^* vs k for case 2. The magnitude of the vorticity is large when $k \ll 1$ and small in the maximum growth region. (c) The two ratios f_l and f_a vs k for case 2. The ratios are high when k is close to 1 but close to 1 when $k \ll 1$ or $k \approx 2$. The maximum value of f_l is 10.37 here, smaller than the value 66.82 in case 1. The reason is that the Reynolds number in case 2 is smaller than in case 1. Both the vorticities and the two ratios could help to understand the good agreement in the maximum growth region and poor agreement when $k \ll 1$ as shown in (a).

exact solution when $k \ll 1$. When the Reynolds number is lower (Figs. 4 and 5) IPF and VPF deviate from the exact solution in the maximum growth region whereas VCVPF can give almost the same maximum growth rate σ_m and the associated wave number k_m as the exact solution. However, VCVPF dose not differ greatly from IPF or VPF when $k \ll 1$. Figure 6 shows the results for case 5 in which the Reynolds number is low and the viscosity ratio $m \sim O(1)$; VCVPF does not give the correct values of σ_m and k_m in this case.

The vorticity as a function of the wave number k helps to understand the nonuniform agreement between the VCVPF results and the exact results. In cases 1, 2, and 3 (Figs. 2–4), the magnitude of the vorticity is large when $k \ll 1$ and small in the maximum growth region. This could explain the good agreement in the maximum growth region and poor agreement when $k \ll 1$. In cases 4 and 5 (Figs. 5 and 6), the magnitude of the vorticity is large at almost all the values of k except when k is very close to $k_c = 2$. The distribution of the vorticity is helpful for understanding the growth rate calculation but a clear explanation for the nonuniform agreement is not obtained in cases 4 and 5.

We find that the values of the two ratios f_l and f_a are close to 1 when $k \ll 1$ in all the cases, indicating that the rotational parts are important for long waves even at high Reynolds number. This is consistent with our growth rate calculation, which shows that the agreement between VCVPF and the exact solution is poor for long waves. In the maximum growth region (k close to 1), the values of f_l and f_a are larger than for long waves. When the Reynolds number is large, the maximum value of f_l and f_a is large, indicating that the irrotational parts dominate the solution; at the same time, we observe good agreement between VCVPF and the exact solution for wave numbers near k_m. When the Reynolds number is small, the values of f_l and f_a are close to 1 in the whole range of k; at the same time, we observe that the agreement between VCVPF and the exact solution is poor at almost all the values of k.

VII. DISSIPATION CALCULATION FOR CAPILLARY INSTABILITY

The dissipation method is a way to include viscous effects into solutions assuming potential flows. Joseph and Wang[10] showed that VCVPF and dissipation method give the same results in a few problems involving free surfaces, such as the drag force on a spherical or oblate ellipsoidal gas bubble and the decay rate of free gravity waves on water. Wang, Joseph, and Funada[9] showed that the dissipation calculation gives the same growth rates as VCVPF for capillary instability involving a gas and a viscous fluid. Here we extend the dissipation calculation to capillary instability of two viscous fluids.

The sum of the mechanical energy equations of the interior and exterior fluids can be written as

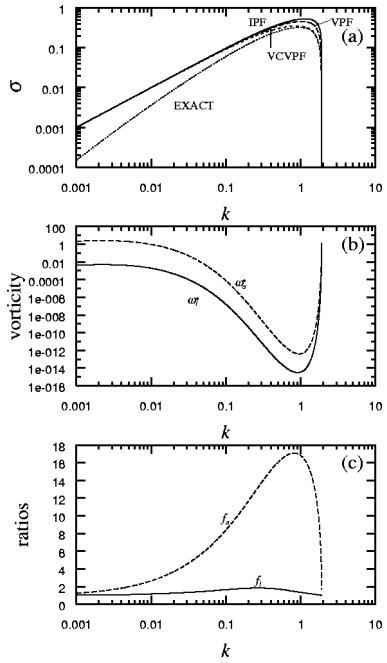

FIG. 4. (a) The growth rate σ vs k for case 3, glycerin in mercury. In the maximum region, IPF and VPF overestimate the growth rate whereas VCVPF gives almost the same value as EXACT. IPF, VPF, and VCVPF deviate from the exact solution considerably when $k \ll 1$. (b) The vorticities ω_l^* and ω_a^* vs k for case 3. The magnitude of the vorticity is large when $k \ll 1$ and small in the maximum growth region. (c) The two ratios f_l and f_a vs k for case 3. The ratios are high when k is close to 1 but close to 1 when $k \ll 1$ or $k \approx 2$. The maximum value of f_l is 1.83, much smaller than in case 1 and case 2. At the same time the Reynolds number is also much smaller than in case 1 and case 2. It is noted that the maximum value of f_a is 17.19, much larger than f_l. The reason is that the value of f_a should correspond to the Reynolds number based on ρ_a and μ_a, which is 2.08×10^7 in case 3. Both the vorticities and the two ratios could help to understand the good agreement in the maximum growth region and poor agreement when $k \ll 1$ as shown in (a).

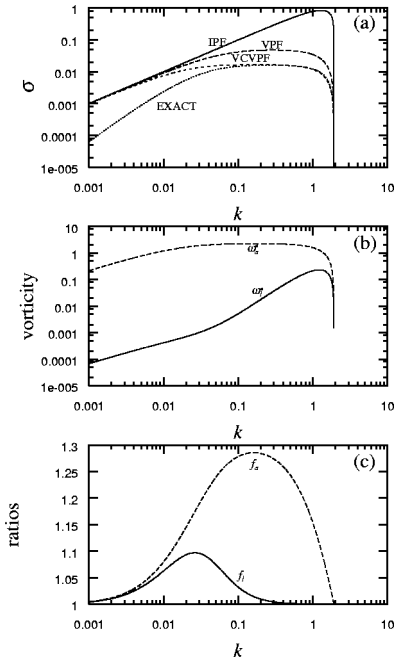

FIG. 5. (a) The growth rate σ vs k for case 4, goldensyrup in paraffin. IPF and VPF deviate from the exact solution considerably in the whole range of $k \leqslant k_c = 2$. VCVPF is still in good agreement with the exact solution in the maximum growth region. (b) The vorticities ω_l^* and ω_a^* vs k for case 4. The magnitude of the vorticity is large at almost all the values of k except when k is very close to $k_c = 2$. (c) The two ratios f_l and f_a vs k for case 4. The maximum value of f_l and f_a does not exceed 1.3, indicating that the rotational parts are important in the whole range of k. This could explain the deviation of IPF and VPF from the exact solution in the whole range. At the same time, the curve for f_a shows that the ratio is higher in the maximum growth region than in the region where $k \ll 1$ or $k \approx 2$. This may help to understand the good agreement between VCVPF and the exact solution in the neighborhood of the maximum growth rate.

$$\frac{d}{dt}\int_{V_a}\frac{\rho_a}{2}|\boldsymbol{u}_a|^2 dV + \frac{d}{dt}\int_{V_l}\frac{\rho_l}{2}|\boldsymbol{u}_l|^2 dV = \int_A [u_n(-p_l + \tau_l^n + p_a - \tau_a^n) + \boldsymbol{u}_l \cdot \boldsymbol{t}\tau_l^s - \boldsymbol{u}_a \cdot \boldsymbol{t}\tau_a^s] dA - \int_{V_a} 2\mu_a \mathbf{D}_a : \mathbf{D}_a dV - \int_{V_l} 2\mu_l \mathbf{D}_l : \mathbf{D}_l dV. \quad (60)$$

We assume that the normal stress balance

$$p_a - \tau_a^n - p_l + \tau_l^n = \frac{\partial^2 \eta}{\partial z^2} + \frac{\eta}{R^2}, \quad (61)$$

and the continuity of the tangential velocity and stress,

$$\tau_a^s = \tau_l^s = \tau^s, \quad \boldsymbol{u}_a \cdot \boldsymbol{t} = \boldsymbol{u}_l \cdot \boldsymbol{t} = u_s, \quad (62)$$

are all satisfied at the interface. At the same time, the flow in the bulk of the fluids are approximated by potential flow, for which the following identity can be easily proved:

$$\int_V 2\mu \mathbf{D}:\mathbf{D}\, dV = \int_A \boldsymbol{n} \cdot 2\mu \mathbf{D} \cdot \boldsymbol{u}\, dA, \quad (63)$$

where A is the surface of V and $\boldsymbol{n}$ is the unit normal pointing outward. Inserting (61)–(63) into (60), we obtain

$$\frac{d}{dt}\int_{V_a}\frac{\rho_a}{2}|\boldsymbol{u}_a|^2 dV + \frac{d}{dt}\int_{V_l}\frac{\rho_l}{2}|\boldsymbol{u}_l|^2 dV = \int_A u_n \gamma\left(\frac{\partial^2 \eta}{\partial z^2} + \frac{\eta}{R^2}\right) dA + \int_A \boldsymbol{n}_1 \cdot 2\mu_a \mathbf{D}_a \cdot \boldsymbol{u}_a dV - \int_A \boldsymbol{n}_1 \cdot 2\mu_l \mathbf{D}_l \cdot \boldsymbol{u}_l dV. \quad (64)$$

The dimensionless form of (64) is

$$l\frac{d}{dt}\int_{V_a}\frac{1}{2}|\boldsymbol{u}_a|^2 dV + \frac{d}{dt}\int_{V_l}\frac{1}{2}|\boldsymbol{u}_l|^2 dV = \int_A u_n\left(\frac{\partial^2 \eta}{\partial z^2} + \frac{\eta}{R^2}\right) dA + \frac{m}{\sqrt{J}}\int_A \boldsymbol{n}_1 \cdot 2\mathbf{D}_a \cdot \boldsymbol{u}_a dA - \frac{1}{\sqrt{J}}\int_A \boldsymbol{n}_1 \cdot 2\mathbf{D}_l \cdot \boldsymbol{u}_l dA. \quad (65)$$

The integrals in (65) are evaluated

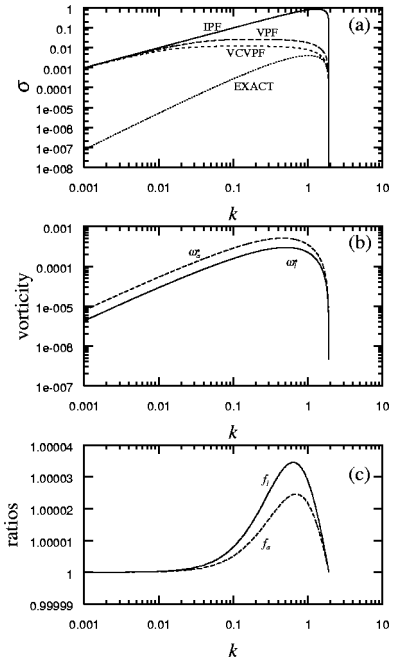

FIG. 6. (a) The growth rate σ vs k for case 5, goldensyrup in BBoil. The agreement between IPF, VPF, and VCVPF with the exact solution is poor at almost all the values of k. (b) The vorticities ω_l^* and ω_a^* vs k for case 5. The magnitude of the vorticity is relatively large at almost all the values of k, and becomes small only when k is very close to $k_c=2$. (c) The two ratios f_l and f_a vs k for case 5. The maximum value of f_l and f_a does not exceed 1.000 035, indicating that the irrotational and rotational parts are almost equally important in the whole range of k. Both the vorticities and the two ratios could help to understand the poor agreement between IPF, VPF, and VCVPF with the exact solution shown in (a).

$$\frac{d}{dt}\int_{V_l}\frac{|\boldsymbol{u}_l|^2}{2}dV=\frac{d}{dt}\int_0^{2\pi}d\theta\int_z^{z+\lambda}\int_0^R\frac{|\boldsymbol{u}_l|^2}{2}r\,dr\,dz$$
$$=|A_1|^2\pi\lambda R^2kI_0(kR)I_1(kR)(\sigma+\overline{\sigma})$$
$$\times\exp(\sigma+\overline{\sigma})t, \tag{66}$$

$$l\frac{d}{dt}\int_{V_a}\frac{|\boldsymbol{u}_a|^2}{2}dV=l\frac{d}{dt}\int_0^{2\pi}d\theta\int_z^{z+\lambda}\int_R^\infty\frac{|\boldsymbol{u}_a|^2}{2}r\,dr\,dz$$
$$=l|B_1|^2\pi\lambda R^2kK_0(kR)K_1(kR)(\sigma+\overline{\sigma})$$
$$\times\exp(\sigma+\overline{\sigma})t, \tag{67}$$

$$\int_A\left(\frac{\partial^2\eta}{\partial z^2}+\frac{\eta}{R^2}\right)u_l dA=2|A_1|^2\pi\lambda R\frac{k^2}{\sigma}I_1^2(kR)$$
$$\times\left(\frac{1}{R^2}-k^2\right)\exp(\sigma+\overline{\sigma})t, \tag{68}$$

$$\frac{1}{\sqrt{J}}\int_A\boldsymbol{n}_1\cdot 2\mathbf{D}_l\cdot\boldsymbol{u}_l dA=\frac{4}{\sqrt{J}}|A_1|^2\pi\lambda Rk^3I_1(kR)\left[2I_0(kR)\right.$$
$$\left.-\frac{I_1(kR)}{kR}\right]\exp(\sigma+\overline{\sigma})t, \tag{69}$$

$$\frac{m}{\sqrt{J}}\int_A\boldsymbol{n}_1\cdot 2\mathbf{D}_a\cdot\boldsymbol{u}_a dA=\frac{4m}{\sqrt{J}}|A_1|^2\pi\lambda Rk^3K_1(kR)\left[2K_0(kR)\right.$$
$$\left.+\frac{K_1(kR)}{kR}\right]\exp(\sigma+\overline{\sigma})t. \tag{70}$$

Inserting (66)–(70) into (65), we obtain

$$(\alpha_l+l\alpha_a)\frac{\sigma+\overline{\sigma}}{2}+\frac{2k^2}{\sqrt{J}}[(\alpha_l+\beta_l)+m(\alpha_a+\beta_a)]$$
$$=\left(\frac{1}{R^2}-k^2\right)\frac{k}{\sigma}, \tag{71}$$

where α_l, α_a, β_a, and β_l are defined in (23). If we assume that σ is real, (71) is the same as the dispersion relation (49) from the VCVPF solution. The solution of the dispersion relation is given in (50). In the range $0<k\leqslant 1/R=2$, σ is real and our assumption is satisfied. Therefore, the growth

TABLE II. Data of the maximum growth rate and the associated wave number.

	IPF		EXACT	
Case	k_m	σ_m	k_m	σ_m
1	1.390 961 6*E*+00	9.637 740 0*E*−01	1.389 398 6*E*+00	9.551 739 9*E*−01
2	1.358 505 0*E*+00	8.958 972 2*E*−01	1.350 889 5*E*+00	8.491 858 5*E*−01
3	1.189 718 1*E*+00	5.573 461 6*E*−01	9.949 639 4*E*−01	3.414 019 4*E*−01
4	1.349 371 6*E*+00	8.750 763 3*E*−01	2.703 269 7*E*−01	1.655 220 8*E*−02
5	1.366 163 4*E*+00	9.130 386 9*E*−01	1.063 202 4*E*+00	4.348 411 6*E*−03
	VPF		VCVPF	
Case	k_m	σ_m	k_m	σ_m
1	1.390 961 6*E*+00	9.633 718 6*E*−01	1.389 398 6*E*+00	9.628 999 2*E*−01
2	1.356 978 5*E*+00	8.932 529 3*E*−01	1.353 930 6*E*+00	8.901 762 5*E*−01
3	1.071 603 0*E*+00	4.757 527 0*E*−01	9.186 273 5*E*−01	3.676 062 9*E*−01
4	2.964 342 9*E*−01	4.873 370 2*E*−02	1.769 323 9*E*−01	1.687 814 1*E*−02
5	2.020 340 3*E*−01	2.757 518 7*E*−02	1.343 316 8*E*−01	1.229 110 3*E*−02

rate computed by the dissipation calculation is the same as that computed by the VCVPF.

VIII. DISCUSSION OF THE PRESSURE CORRECTIONS AT THE INTERFACE OF TWO VISCOUS FLUIDS

Our pressure corrections arise in a boundary layer induced by the discontinuity of the tangential velocity and shear stress at the interface evaluated using the potential solution. We assume that the boundary layer is thin and when the boundary layer is considered, the tangential velocity and shear stress are continuous at the interface. This assumption leads to good agreements between the exact solution and VCVPF for the liquid–gas cases and less good agreements, better than what might be expected, in the cases of two fluids for which the boundary layer assumptions do not hold uniformly and will be discussed in this section. In the boundary layer near the interface, we divide the velocity and pressure into irrotational part and viscous correction part,

$$u = u^i + u^v, \quad w = w^i + w^v, \quad p = p^i + p^v. \tag{72}$$

The irrotational tangential velocities at the interface are

$$w_l^i = -A_1 k I_0(kR)\exp(\sigma t + ikz), \tag{73}$$

$$w_a^i = A_1 k \frac{I_1(kR)}{K_1(kR)} K_0(kR)\exp(\sigma t + ikz). \tag{74}$$

The tangential stresses at the interface evaluated using the potential flows are

$$\tau_l^s = -(2/\sqrt{J})A_1 k^2 I_1(kR)\exp(\sigma t + ikz), \tag{75}$$

$$\tau_a^s = -(2m/\sqrt{J})A_1 k^2 I_1(kR)\exp(\sigma t + ikz). \tag{76}$$

The continuity of the tangential velocity requires

$$w_l^i + w_l^v = w_a^i + w_a^v, \tag{77}$$

which gives rise to

$$w_l^v - A_1 k I_0(kR)\exp(\sigma t + ikz) = w_a^v + A_1 k \frac{I_1(kR)}{K_1(kR)} K_0(kR) \times \exp(\sigma t + ikz). \tag{78}$$

If we assume $w_a^v = q w_l^v$, (78) can be written as

$$w_l^v(1-q) = A_1 k\left[I_0(kR) + \frac{I_1(kR)}{K_1(kR)} K_0(kR) \right]\exp(\sigma t + ikz). \tag{79}$$

The continuity of the shear stress requires

$$\frac{1}{\sqrt{J}}\left(\frac{\partial u_l^v}{\partial z} + \frac{\partial w_l^v}{\partial r} \right) - \frac{2}{\sqrt{J}} A_1 k^2 I_1(kR)\exp(\sigma t + ikz) = \frac{m}{\sqrt{J}}\left(\frac{\partial u_a^v}{\partial z} + \frac{\partial w_a^v}{\partial r} \right) - 2\frac{m}{\sqrt{J}} A_1 k^2 I_1(kR)\exp(\sigma t + ikz). \tag{80}$$

Since the potential flow solution satisfies the continuity of the normal velocity $u_l^i = u_a^i$, the viscous corrections to the normal velocity in the boundary layer should be very small. Thus $\partial u_l^v/\partial z$ and $\partial u_a^v/\partial z$ can be ignored and (80) becomes

$$\frac{\partial}{\partial r}(w_l^v - m w_a^v) = 2(1-m)A_1 k^2 I_1(kR)\exp(\sigma t + ikz). \tag{81}$$

Assuming that the boundary layer thickness δ is small, we can write (81) approximately as

$$w_l^v(1-mq)/\delta = 2(1-m)A_1 k^2 I_1(kR)\exp(\sigma t + ikz). \tag{82}$$

Comparing (79) and (82), we obtain

$$\frac{1-mq}{(1-q)(1-m)}\frac{1}{\delta} = \frac{2kI_1(kR)}{I_0(kR) + I_1(kR)\dfrac{K_0(kR)}{K_1(kR)}}. \tag{83}$$

Therefore, (83) needs to be satisfied if the continuities of the tangential velocity and stress are to be enforced. In other words, the assumptions on which VCVPF is based are valid only if (83) is satisfied. Since we do not solve the boundary layer problem, q and δ are unknown and we are not able to determine if (83) is satisfied. However, we may assume that δ is very small and estimate the possibility of satisfying (83) under different conditions, i.e., different values of m and k. We have the following observations regarding (83).

(1) Since δ is supposed to be small, (83) is easier to satisfy when the right-hand side is larger. Calculation shows that the right-hand side of (83) is 5×10^{-7} when $k=0.001$ and is 1.36 when $k=2$. Therefore, (83) can be satisfied for k close to $k_c=2$ but is very difficult to satisfy for small k. This observation could help to understand the results of the growth rate calculation, i.e., the agreement between VCVPF and the exact solution is good for k close to k_c but is poor when $k \ll 1$.

(2) The term on the left-hand side of (83)

$$\frac{1-mq}{(1-q)(1-m)} \tag{84}$$

should be comparable to or even smaller than δ, so that (83) can be satisfied. We find that for certain values of q, (84) is small when m is much smaller than 1 and is large when m is close to 1. For example, if we fix q at 10, the value of (84) is 0.0125 when $m=0.11$ and is 8.89 when $m=0.9$. This observation may help to understand our growth rate calculation at low Reynolds numbers. In case 4, $m=3.091\times10^{-4}$ and VCVPF is in good agreement with the exact solution in the region of maximum growth; in case 5, $m=0.5455$ and VCVPF does not give the correct maximum growth rate σ_m and the associated wave number k_m. The value of m does not seem to be important at high Reynolds numbers. In cases 1 and 2, IPF, VPF, VCVPF all agree well with the exact solution in the region of maximum growth even when the value of m is relatively close to 1. This is because the boundary layer and the viscous correction are not important at high Reynolds numbers.

We have shown that the condition (83) can be satisfied in some cases (k close to $k_c=2$ and $m \ll 1$), and is very difficult to satisfy in other cases ($k \ll 1$ or m close to 1). When (83) is satisfied, the assumption of continuous tangential velocity and stress is realized approximately and our calculation does show good agreement between VCVPF and VPF. When (83)

is difficult to satisfy, VCVPF may not give a good approximation to the exact solution, especially at low Reynolds numbers. Thus, viscous potential flows with pressure corrections can be used to approximate viscous flows in problems involving the interface of two viscous fluids, but this approximation is not uniformly valid.

When the viscous corrections for the velocity and pressure are added to the irrotational flow, the complete form of the normal stress balance is

$$p_a^i + p_a^v - p_l^i - p_l^v + \frac{2}{\sqrt{J}}\left(\frac{\partial u_l^i}{\partial r} + \frac{\partial u_l^v}{\partial r}\right) - \frac{2m}{\sqrt{J}}\left(\frac{\partial u_a^i}{\partial r} + \frac{\partial u_a^v}{\partial r}\right) = \frac{\partial^2 \eta}{\partial z^2} + \frac{\eta}{R^2}. \tag{85}$$

The viscous corrections of the velocity satisfy the continuity equation

$$\frac{\partial u_l^v}{\partial r} + \frac{u_l^v}{r} + \frac{\partial w_l^v}{\partial z} = 0. \tag{86}$$

We may estimate the order of the terms in (86),

$$2\frac{u_l^v}{\delta} \sim \frac{w_l^v}{\lambda}. \tag{87}$$

Combining (82) and (87), we obtain

$$\frac{\partial u_l^v}{\partial r} \sim \frac{u_l^v}{\delta} \sim \frac{\delta}{\lambda}\frac{1-m}{1-mq}A_1 k^2 I_1(kR). \tag{88}$$

At the same time, we have

$$\frac{\partial u_l^i}{\partial r} \sim A_1 k^2\left(I_0(kR) - \frac{I_1(kR)}{kR}\right). \tag{89}$$

If $(1-m)/(1-mq)$ is not a very big value, $\partial u_l^v/\partial r$ may be significantly smaller than $\partial u_l^i/\partial r$. A similar argument can show that $\partial u_a^v/\partial r$ could be significantly smaller than $\partial u_a^i/\partial r$. Therefore, $\partial u_l^v/\partial r$ and $\partial u_a^v/\partial r$ can be ignored in (85) and we obtain the normal stress balance equation (40) used in VCVPF calculation. Admittedly, omission of $\partial u_l^v/\partial r$ and $\partial u_a^v/\partial r$ is not justified for certain values of m and q, which may be partially responsible for the poor agreement between VCVPF and the exact solution in some cases.

IX. CONCLUSIONS

A method for computing a viscous correction of viscous potential flow is derived for problems in which the interface of two fluids is involved and the flows of the two fluids are assumed to be irrotational. The potential flow solution $\boldsymbol{u} = \nabla\phi$, $\nabla^2\phi = 0$ generally cannot satisfy the zero-shear-stress condition at gas–liquid interfaces or the continuity of the tangential velocity and shear stress at liquid–liquid interfaces. We assume that the flow can be approximated by a thin boundary layer near the interface and potential flow in the bulk liquids. Within this boundary layer, all the physical boundary conditions are satisfied. The velocity and pressure fields in the boundary layer can be decomposed into viscous and potential parts, where the potential part is already known. Substitution of this decomposition into the Navier–Stokes equations gives rise to equations for unknown viscous pressure and velocity fields. This procedure is similar to the analysis of Moore,[16] Prosperetti,[17] and Kang and Leal.[18] However, our method is simpler because the viscous part of the velocity field in the boundary layer is not needed since the leading order direct effects are accommodated by the viscous part of the normal stress evaluated on the irrotational motion, but the viscous part of the pressure at the interface is of the same order as the irrotational normal stress and it is needed. The linearized equations coupling the viscous part of the solenoidal velocity field to the viscous part of the pressure imply that this pressure is harmonic. The Laplace equation for this is solved to obtain the viscous pressure field in the form of a harmonics series with arbitrary coefficients. For nonlinear problems, the viscous pressure at the interface is expanded directly in a surface harmonics series with arbitrary coefficients. To determine the arbitrary coefficients, we formulate two mechanical energy equations using (1) VPF and (2) VCVPF, respectively. In case (1), only the potential flow solutions are used in the mechanical energy equation giving rise to a relation which equates the volume integrals of the dissipation and the rate of change of kinetic energy to the power of the normal and tangential tractions exerted by the potential flows on either side of the interface. In case (2), the potential flow with the viscous correction of the pressure which arises in the boundary layer appears at the interface in the traction integral that appears in the mechanical energy equation. The tangential velocities and stresses are continuous and no terms due to tractions from the shear stresses appear. The viscous normal stress arising from the viscous component of the velocity field in the boundary layer is assumed to be small and neglected. For example, in the analysis of the decay of free gravity waves, Joseph and Wang[10] showed that this extra viscous normal stress is in the order of the boundary layer thickness δ and negligible. The power due to the normal tractions then includes contributions from the pressure and viscous normal stress evaluated using the potential solutions and from the extra viscous pressure. We assume the boundary layer is so thin that the volume integrals inside the boundary layer are negligible compared to those in the bulk liquids. Therefore, the volume integrals of the dissipation and the rate of change of kinetic energy are approximately equal to those evaluated using potential flow solutions. Comparing the above two mechanical energy equations, one finds that the power due to the traction of the extra viscous pressure at the interface is equal to the power due to the tangential traction of the irrotational shear stresses. This relation is then used to determine the coefficient of the principal mode in the harmonic series expression for the extra viscous pressure; the principal mode is defined as the mode matched to the velocity potential. The principle mode of the extra viscous pressure is then determined and can be used in calculations of the hydrodynamics for the problem, such as the normal stress balance at the interface in capillary instability and the direct calculation of drag on bubbles and drops.

This viscous pressure correction is applied to capillary instability and gives rise to growth rate curves closer to the exact solution than inviscid or viscous potential flow. The

viscous correction of the pressure leads to an excellent approximation of the exact solution, uniform in the wave number, when one of the two fluids is a gas. For two viscous liquids the approximation of the maximum growth rates is reasonable to good but the long waves are not well approximated. The nonuniform improvements which we get with pressure corrections at liquid–liquid interfaces is unanticipated. Unlike the free surface problems in which the boundary layer is considered to be weak, the boundary layer near a liquid–liquid interface is often the major source of the viscous dissipation of the flow, and the irrotational flow solution is considered to be a very poor approximation to the exact solution. However, our analysis shows that viscous potential flows with pressure corrections can approximate the exact solution in some cases, even though the approximation is not uniformly valid.

Our pressure corrections arise in a boundary layer induced by the discontinuity of the tangential velocity and shear stress at the interface evaluated using the potential solution. We assume that the boundary layer is thin and when the boundary layer is considered, the tangential velocity and shear stress are continuous at the interface. We find that in the problem of capillary instability, this assumption is difficult to satisfy for long waves but is possible to satisfy near the region of maximum growth. This observation helps to explain why the approximation using the pressure correction is not uniform in the wave number. We evaluate the vorticity using the exact solution; when the vorticity is great, viscous potential flow with a pressure correction does not give a uniformly good approximation. We divide the stream functions of the exact solution into irrotational and rotational parts; the ratio of the irrotational part to the rotational part is computed. Larger ratios indicate that the irrotational parts dominate the solution and potential flow can give a good approximation. Both the vorticity and the ratio calculation are helpful in understanding the nonuniform improvement by the pressure correction.

We carry out dissipation calculation for capillary instability of two fluids. The growth rates from dissipation calculations are the same as those from viscous potential flow with pressure corrections.

ACKNOWLEDGMENT

This work was supported in part by a grant from NSF/CTS.

[1] L. Rayleigh, "On the capillary phenomena of jets," Proc. R. Soc. London **29**, 71 (1879).
[2] J. A. F. Plateau, *Statique experimentale et theorique des liquide soumis aux seules forces moleculaire* (Gauthier–Villars, Paris, 1873), Vol. ii, p. 231.
[3] L. Rayleigh, "On the instability of a cylinder of viscous liquid under capillary force," Philos. Mag. **34**, 145 (1892).
[4] C. Weber, "Zum Zerfall eines Flüssigkeitsstrahles," Z. Angew. Math. Mech. **11**, 136 (1931).
[5] S. Chandrasekhar, *Hydrodynamic and Hydromagnetic Stability* (Oxford University Press, Oxford, 1961).
[6] J. Eggers, "Nonlinear dynamics and breakup of free-surface flows," Rev. Mod. Phys. **69**, 865 (1997).
[7] S. Tomotika, "On the instability of a cylindrical thread of a viscous liquid surrounded by another viscous fluid," Proc. R. Soc. London **150**, 322 (1935).
[8] T. Funada and D. D. Joseph, "Viscous potential flow analysis of capillary instability," Int. J. Multiphase Flow **28**, 1459 (2002).
[9] J. Wang, D. D. Joseph, and T. Funada, "Pressure correction for potential flow analysis of capillary instability of viscous fluids," J. Fluid Mech. **522**, 383 (2005).
[10] D. D. Joseph and J. Wang, "The dissipation approximation and viscous potential flow," J. Fluid Mech. **505**, 365 (2004).
[11] H. Lamb, *Hydrodynamics*, 6th ed. (Cambridge University Press, Cambridge, 1932) (reprinted by Dover, New York, 1945).
[12] C. A. Miller and L. E. Scriven, "The oscillations of a droplet immersed in another fluid," J. Fluid Mech. **32**, 417 (1968).
[13] A. Prosperetti, "Normal-mode analysis for the oscillations of a viscous liquid drop in an immiscible liquid," J. Mec. **19**, 149 (1980).
[14] T. S. Lundgren and N. N. Mansour, "Oscillations of drops in zero gravity with weak viscous effects," J. Fluid Mech. **194**, 479 (1988).
[15] R. M. Christiansen and A. N. Hixson, "Breakup of a liquid jet in a denser liquid," Ind. Eng. Chem. **49**, 1017 (1957).
[16] D. W. Moore, "The boundary layer on a spherical gas bubble," J. Fluid Mech. **16**, 161 (1963).
[17] A. Prosperetti, "Viscous effects on small-amplitude surface waves," Phys. Fluids **19**, 195 (1976).
[18] I. S. Kang and L. G. Leal, "Small-amplitude perturbations of shape for a nearly spherical bubble in an inviscid straining flow (steady shapes and oscillatory motion)," J. Fluid Mech. **187**, 231 (1988).